and is applicable even to large discontinuities. The present method is especially powerful to analyze the radiation characteristics due to the discontinuity. If we can ignore the radiation wave, the transmission and the reflection powers can be obtained very easily by the least squares boundary residual method.

ACKNOWLEDGMENT

The authors wish to thank Prof. M. Matsuhara and Dr. N. Morita of Osaka University for their valuable discussions, and W. Uchida of Nippon Electric Company for his cooperation in carrying out the numerical computations.

REFERENCES

[1] D. L. Bisbee, "Measurements of loss due to offsets and end separations of optical fibers," *Bell Syst. Tech. J.*, vol. 50, no. 10, p. 3159, Dec. 1971.
[2] L. G Cohen, "Power coupling from GaAs injection lasers into optical fibers," *Bell Syst. Tech. J.*, vol. 51, no. 3, p. 573, Mar. 1972.
[3] J. S. Cook, W. L. Mammel, and R. J. Grow, "Effect of misalignments on coupling efficiency of single-mode optical fiber butt joints," *Bell Syst. Tech. J.*, vol. 52, no. 8, p. 1439, Oct. 1973.
[4] T. Sekizawa, "Components for optical-fiber transmission," *J. Inst. Electron. Commun. Eng. Japan*, vol. 59, no. 7, p. 728, July 1976.
[5] T. C. Chu and A. R. McCormick, "Measurements of loss due to offset, end separation, and angular misalignment in graded index fibers excited by an incoherent source," *Bell Syst. Tech. J.*, vol. 57, no. 3, p. 595, Mar. 1978.
[6] S. F. Mahmoud and J. C. Beal, "Scattering of surface waves at a dielectric discontinuity on a planar waveguide," *IEEE Trans. Microwave Theory Tech.*, vol. MTT-23, p. 193, Feb. 1975.
[7] D. Marcuse, "Radiation losses of tapered dielectric slab waveguides," *Bell Syst. Tech. J.*, vol. 49, no. 2, p. 273, Feb. 1970.
[8] B. Rulf, "Discontinuity radiation in surface waveguides," *J. Opt. Soc. Amer.*, vol. 65, no. 11, p. 1248, Nov. 1975.
[9] G. H. Brooke and M. M. Z. Kharadly, "Step discontinuities on dielectric waveguides," *Electron. Lett.*, vol. 12, no. 18, p. 473, Sept. 1976.
[10] D. Gloge, "Offset and tilt loss in optical fiber splices," *Bell Syst. Tech. J.*, vol. 55, no. 7, p. 905, Sept. 1976.
[11] C. M. Miller, "Transmission vs transverse offset for parabolic-profile fiber splices with unequal core diameters," *Bell Syst. Tech. J.*, vol. 55, no. 7, p. 917, Sept. 1976.
[12] J. B. Davies, "A least-squares boundary residual method for the numerical solution of scattering problems," *IEEE Trans. Microwave Theory Tech.*, vol. MTT-21, p. 99, Feb. 1973.
[13] H. Oraizi and J. Perini, "A numerical method for the solution of the junction of cylindrical waveguides," *IEEE Trans. Microwave Theory Tech.*, vol. MTT-21, p. 640, Oct. 1973.

# Computer-Aided Design of *H*-Plane Waveguide Junctions with Full-Height Ferrites of Arbitrary Shape

NAOMICHI OKAMOTO, MEMBER, IEEE

***Abstract*—A method for solving the problem of *H*-plane waveguide junctions with a full-height ferrite post of arbitrary shape is proposed. The junctions are allowed to have arbitrary cross section and arbitrary number of ports. The method is based on the integral equations derived from the reciprocity theorems in both the ferrite region and the air region ranging from the reference planes of connecting waveguides to the inside of the junction.**

**For comparison with the previously published experimental and theoretical results, Y junctions with a circular ferrite post are first treated. Excellent agreement has been found between the experimental data and the numerical results obtained by the present method.**

**The performance of a Y-junction circulator with a triangular ferrite post having rounded angles is next investigated. Both the ferrite geometry and the internal dc magnetic field are examined in detail. For this geometry the calculated 20-dB bandwidth has been found to become greater as the cross section of the ferrite approaches a regular triangle from a circle.**

Manuscript received September 21, 1977; revised August 7, 1978.
The author is with the Department of Electronic Engineering, Shizuoka University, Johoku, Hamamatsu, Japan.

## I. INTRODUCTION

A VERSATILE waveguide junction which is now in wide use is the ferrite junction circulator. The waveguide Y-junction circulator was first proposed by Chait and Curry [1]. Davies [2] presented the theoretical treatment for a symmetrical waveguide junction circulator with a circular ferrite post, including a detailed field analysis inside the junction. This method was extended to junctions with coaxial composite ferrite posts which produced much larger bandwidths [3]–[5]. In these analyses, only the dominant-mode fields in the waveguides were approximately matched to a summation of mode fields within the junction. This neglect of the higher modes is the reason for the discrepancy between the numerical results and the experimental measurements. Later, this defect was improved by adding the higher modes [6] and by using the point-matching technique, and at the same

0018-9480/79/0400-0315$00.75 

time the latter method was extended to the asymmetrical junctions [7]. Recently, the point-matching method was applied to the junctions with a triangular ferrite post [8]. Moreover, accompanied with recent progress in computer analysis, the integral equation method [9], [10] was applied to the problems of planar circuits having an arbitrary shape [11].

This paper presents a method for solving the problem of $H$-plane waveguide junctions with a full-height ferrite post of arbitrary shape. The junctions are allowed to have an arbitrary cross section and arbitrary number of ports. The method is based on the integral equations derived from the reciprocity theorems in both the ferrite region and the air region ranging from the reference planes of connecting waveguides to the inside of the junction. Making use of the method, we first treat Y junctions with a circular ferrite post for comparison with the previously published experimental [5] and theoretical results [5], [7]. The performance of Y-junction circulators with a triangular ferrite post having rounded angles is next investigated. The influences of both the ferrite geometry and the dc magnetic field on the performance are examined.

## II. Formulation

Fig. 1(a) shows the $H$-plane waveguide junction of $N^p$-ports with a full-height ferrite post of arbitrary shape. It is assumed that the junction geometry and the electromagnetic fields with the time dependence $e^{j\omega t}$ are constant along the $z$ axis. Moreover, the waveguides propagate only the dominant $TE_{10}$ mode, while all higher modes are cutoff. The reference plane of each port is selected so far from the junction that the fields there are due only to the dominant mode. However, this does not mean that the higher modes in the waveguides are neglected. Those are considered as surface currents on the waveguide walls in the following analysis. The dc magnetic field is applied in parallel with the $z$ axis.

Maxwell's equations in the region $S^f$ occupied by the ferrite post are $\nabla\times\boldsymbol{E}^f=-j\omega\bar{\mu}\cdot\boldsymbol{H}^f$ and $\nabla\times\boldsymbol{H}^f=j\omega\epsilon\boldsymbol{E}^f$, where $\boldsymbol{E}^f$ and $\boldsymbol{H}^f$ are the total electric and magnetic fields inside the ferrite, and $\bar{\mu}$ and $\epsilon$ are the tensor permeability and the permittivity of the ferrite, respectively. Suppose that the medium characterized by the transposed tensor permeability $\tilde{\mu}$ and the permittivity $\epsilon$ occupies the whole space as in Fig. 1(b), and that an auxiliary electric line source $\tilde{J}_z(\boldsymbol{r})=\delta(\boldsymbol{r}-\bar{\boldsymbol{r}})$ located at $\bar{\boldsymbol{r}}$ in the complementary region $\tilde{S}^f$ (i.e., $\tilde{S}^f+S^f=$whole space) generates the fields $\tilde{\boldsymbol{E}}^f$ and $\tilde{\boldsymbol{H}}^f$. Here $\boldsymbol{r}=(r,\phi)$ and $\bar{\boldsymbol{r}}=(\bar{r},\bar{\phi})$ are the radius vectors in the $xy$ plane, and $\delta$ is the Dirac's delta function. We have then a relation $\nabla\cdot(\boldsymbol{E}^f\times\tilde{\boldsymbol{H}}^f-\tilde{\boldsymbol{E}}^f\times\boldsymbol{H}^f)=0$ in region $S^f$, and, hence, the integral yields

$$\oint_{C^f}\left[E_z^f(\boldsymbol{r})\tilde{H}_l^f(\boldsymbol{r},\bar{\boldsymbol{r}})-\tilde{E}_z^f(\boldsymbol{r},\bar{\boldsymbol{r}})H_l^f(\boldsymbol{r})\right]dl=0,\qquad \boldsymbol{r}\in C^f,\bar{\boldsymbol{r}}\in\tilde{S}^f \quad (1)$$

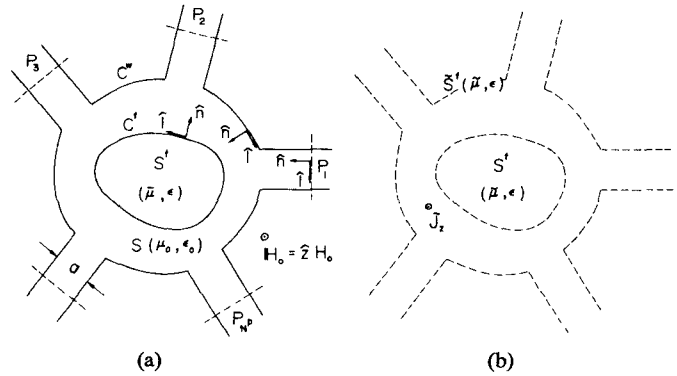


Fig. 1. (a) Cross section of $H$-plane waveguide junction with full-height ferrite post of arbitrary shape. (b) Auxiliary source in the transposed medium of infinite extent.

where $C^f$ is the ferrite air boundary, the subscripts $z$ and $l$ denote the $z$ and circumferential components, respectively, and $(n,l,z)$ is a right-handed orthogonal Cartesian coordinate system with $\hat{n}\times\hat{l}=\hat{z}$. The auxiliary fields are written as [12]

$$\tilde{E}_z^f(\boldsymbol{r},\bar{\boldsymbol{r}})=-(\omega\mu_{\text{eff}}/4)H_0^{(2)}(k_f|\boldsymbol{r}-\bar{\boldsymbol{r}}|)$$
$$\tilde{H}_l^f(\boldsymbol{r},\bar{\boldsymbol{r}})=(j/4)(\partial/\partial n-j\mu_q\partial/\partial l)H_0^{(2)}(k_f|\boldsymbol{r}-\bar{\boldsymbol{r}}|) \quad (2)$$

where $\mu_q=\kappa/\mu$, $\mu_{\text{eff}}=\mu(1-\mu_q^2)$, $\mu$ and $\kappa$ are the diagonal and off-diagonal elements of the tensor permeability $\bar{\mu}$, respectively, $k_f=\omega(\mu_{\text{eff}}\epsilon)^{1/2}=k_r k$, $k=\omega(\mu_0\epsilon_0)^{1/2}$, $k_r=(\mu_{\text{eff}}\epsilon_r/\mu_0)^{1/2}$, and $\epsilon_r=\epsilon/\epsilon_0$. Furthermore, $H_0^{(2)}$ is the Hankel function of the second kind of order zero, and $\partial/\partial n$ and $\partial/\partial l$ refer to the normal and circumferential differential operators, respectively.

The region $S$ is surrounded by the boundary $C^f$, all the reference planes $P_i$ $(i=1,2,\cdots,N^p)$, and the conductive walls $C^w$ ranging from the junction to the reference planes as shown in Fig. 1(a). Let $\boldsymbol{E}$ and $\boldsymbol{H}$ be the total fields in region $S$. The similar procedures as those in region $S^f$ give $\nabla\cdot(\boldsymbol{E}\times\tilde{\boldsymbol{H}}-\tilde{\boldsymbol{E}}\times\boldsymbol{H})=0$ in region $S$ where the auxiliary source $\tilde{J}_z$ located in the complementary region $\tilde{S}$ of $S$ generates $\tilde{\boldsymbol{E}}$ and $\tilde{\boldsymbol{H}}$ in free space. Considering the boundary conditions on the conductive walls $C^w$ and the boundary $C^f$, the integral yields

$$\sum_{n=1}^{N^p}\int_{P_n}\left[E_z(\boldsymbol{r})\tilde{H}_l(\boldsymbol{r},\bar{\boldsymbol{r}})-\tilde{E}_z(\boldsymbol{r},\bar{\boldsymbol{r}})H_l(\boldsymbol{r})\right]dl$$
$$-\int_{C^w}\tilde{E}_z(\boldsymbol{r},\bar{\boldsymbol{r}})H_l(\boldsymbol{r})\,dl$$
$$+\int_{C^f}\left[E_z^f(\boldsymbol{r})\tilde{H}_l(\boldsymbol{r},\bar{\boldsymbol{r}})-\tilde{E}_z(\boldsymbol{r},\bar{\boldsymbol{r}})H_l^f(\boldsymbol{r})\right]dl=0,\qquad \bar{\boldsymbol{r}}\in\tilde{S} \quad (3)$$

where $\tilde{E}_z$ and $\tilde{H}_l$ are given by replacing $\mu_{\text{eff}}$ with $\mu_0$, $\mu_q$ with zero, and $k_f$ with $k$ in the respective expressions of (2).

We now expand the unknown tangential electric and magnetic fields in (1) and (3) as follows:

$$H_l(\boldsymbol{r}) = \sum_{n=1}^{N^w} J_n P_n(\boldsymbol{r}), \qquad \boldsymbol{r} \in C^w \tag{4}$$

$$\left.\begin{aligned} H_l^f(\boldsymbol{r}) &= \sum_{n=1}^{N^f} J_n^f T_n(\boldsymbol{r}) \\ E_z^f(\boldsymbol{r}) &= \sum_{n=1}^{N^f} K_n^f T_n(\boldsymbol{r}) \end{aligned}\right\}, \qquad \boldsymbol{r} \in C^f \tag{5}$$

$$\left.\begin{aligned} E_z(\boldsymbol{r}) &= V_n g_n(\boldsymbol{r}) \\ H_l(\boldsymbol{r}) &= -I_n g_n(\boldsymbol{r}) \end{aligned}\right\}, \qquad \boldsymbol{r} \in P_n \ (n = 1,2,\cdots,N^p) \tag{6}$$

where $J_n$, $J_n^f$, $K_n^f$, and $I_n$ are the expansion coefficients to be determined, and $V_n$ are the coefficients given in the following. The respective boundaries $C^w$ and $C^f$ are divided equally into $N^w$ and $N^f$ subsections, that is, $\Delta C_i^w$ $(i = 1,2,\cdots,N^w)$ and $\Delta C_i^f$ $(i = 1,2,\cdots,N^f)$. The pulse function $P_n(\boldsymbol{r})$ in (4) equals 1 on $\Delta C_n^w$ and 0 on $\Delta C_m^w$ $(m \neq n)$. The triangle function $T_n(\boldsymbol{r})$ in (5) has the shape of an isosceles triangle with the vertex value 1; that is, $T_n = 1 - |l - l_n|/\Delta^f$ only on $\Delta C_n^f + \Delta C_{n+1}^f$ and $T_n = 0$ on the other subsections where $l$ is the circumferential length along contour $C^f$, $l_n$ is that value for the boundary point of $\Delta C_n^f$ and $\Delta C_{n+1}^f$, and $\Delta^f$ is the arc length of the subsections on $C^f$. The linear combinations of $P_n$ and $T_n$ in (4) and (5) give a step approximation to $H_l$ on $C^w$ and piecewise linear approximations to $H_l^f$ and $E_z^f$ on $C^f$, respectively. For the gyrotropic bodies, the triangle functions were found to yield extremely better convergence of the solution than the pulse functions [13]. The function $g_n(\boldsymbol{r})$ in (6) represents the pattern of the transverse fields for the dominant mode across the waveguide axis, so that the incoming complex power from the $n$th-port equals $(ab/4)V_n I_n^*$. Here an asterisk denotes the complex conjugate, and $a$ and $b$ are the width and height of the waveguide, respectively. If $\boldsymbol{V}$ and $\boldsymbol{I}$ are column vectors with the respective elements $V_n$ and $I_n$, then $\boldsymbol{I} = [Y]\boldsymbol{V}$ defines the admittance matrix $[Y]$. The fields within the region $S$ and $S^f$ are uniquely specified by giving the tangential electric fields over all the reference planes, namely, the vector $\boldsymbol{V}$ [14]. Therefore, we derive the matrix formulation for determining the vectors $\boldsymbol{I}$, $\boldsymbol{J}$, $\boldsymbol{J}^f$, and $\boldsymbol{K}^f$ and the matrix $[Y]$ for the given vector $\boldsymbol{V}$ where $\boldsymbol{J}$, $\boldsymbol{J}^f$, and $\boldsymbol{K}^f$ are column vectors with elements $J_n$, $J_n^f$, and $K_n^f$, respectively. The numbers $N_t$ of all the unknowns then equal $(2N^f + N^w + N^p)$.

Equations (4)–(6) are now substituted into (1) and (3). We then allow the point $\bar{r}$ in (1) to approach the boundary point $\bar{r}_m^f$ of $\Delta C_m^f$ and $\Delta C_{m+1}^f$ from region $\tilde{S}^f$ $(m = 1,2,\cdots,N^f)$. Similarly, from region $\tilde{S}$ the point $\bar{r}$ in (3) is brought near to $\bar{r}_m^f$ $(m = 1,2,\cdots,N^f)$, the midpoint $\bar{r}_m^w$ of $\Delta C_m^w$ $(m = 1,2,\cdots,N^w)$, and the midpoint $\bar{r}_m^p$ of the port $P_m$ $(m = 1,2,\cdots,N^p)$. Hence, if $V_i = 1$ and the other elements $V_j = 0$ (the vector $\boldsymbol{I}$ then reduces to the $i$th column of the matrix $[Y]$), the following simultaneous matrix equations of the $N_t$th order are obtained:

$$\begin{bmatrix} [E_{mn}^{pp}] & [E_{mn}^{pw}] & [E_{mn}^{pf}] & [H_{mn}^{pf}] \\ [E_{mn}^{wp}] & [E_{mn}^{ww}] & [E_{mn}^{wf}] & [H_{mn}^{wf}] \\ [E_{mn}^{fp}] & [E_{mn}^{fw}] & [E_{mn}^{ff}] & [H_{mn}^{ff}] \\ [0] & [0] & [\hat{E}_{mn}^{ff}] & [\hat{H}_{mn}^{ff}] \end{bmatrix} \begin{bmatrix} \boldsymbol{I} \\ \boldsymbol{J} \\ \boldsymbol{J}^f \\ \boldsymbol{K}^f \end{bmatrix} = \begin{bmatrix} \boldsymbol{G}_i^p \\ \boldsymbol{G}_i^w \\ \boldsymbol{G}_i^f \\ \boldsymbol{O} \end{bmatrix} \tag{7}$$

where $\boldsymbol{G}_i^s$ $(s = p, w, \text{and } f)$ is a column vector with elements $G_{im}^s$ of number $N^s$,

$$G_{im}^s = -\int_{P_i} g_i(\boldsymbol{r}) \tilde{H}_l(\boldsymbol{r},\bar{r})\, dl \tag{8}$$

$$E_{mn}^{sp} = \int_{P_n} g_n(\boldsymbol{r}) \tilde{E}_z(\boldsymbol{r},\bar{r})\, dl, \qquad n = 1,2,\cdots,N^p \tag{9}$$

$$E_{mn}^{sw} = -\int_{\Delta C_n^w} \tilde{E}_z(\boldsymbol{r},\bar{r})\, dl, \qquad n = 1,2,\cdots,N^w \tag{10}$$

$$E_{mn}^{sf} = -\int_{\Delta C_n^f + \Delta C_{n+1}^f} T_n(\boldsymbol{r}) \tilde{E}_z(\boldsymbol{r},\bar{r})\, dl, \qquad n = 1,2,\cdots,N^f \tag{11}$$

$$H_{mn}^{sf} = \int_{\Delta C_n^f + \Delta C_{n+1}^f} T_n(\boldsymbol{r}) \tilde{H}_l(\boldsymbol{r},\bar{r})\, dl, \qquad n = 1,2,\cdots,N^f \tag{12}$$

and where the point $\bar{r}$ in (8)–(12) is brought near to $\bar{r}_m^s$ $(m = 1,2,\cdots,N^s;\ s = p, w, \text{and } f)$ from region $\tilde{S}$. Furthermore,

$$\left.\begin{aligned} \hat{E}_{mn}^{ff} &= -\int_{\Delta C_n^f + \Delta C_{n+1}^f} T_n(\boldsymbol{r}) \tilde{E}_z^f(\boldsymbol{r},\bar{r})\, dl \\ \hat{H}_{mn}^{ff} &= \int_{\Delta C_n^f + \Delta C_{n+1}^f} T_n(\boldsymbol{r}) \tilde{H}_l^f(\boldsymbol{r},\bar{r})\, dl \end{aligned}\right\} \quad \begin{matrix} \bar{r} \in \tilde{S}^f \to \bar{r}_m^f \\ m,n = 1,2,\cdots,N^f. \end{matrix} \tag{13, 14}$$

[0] is a null matrix, and $\boldsymbol{O}$ is a null column vector. The detailed expressions of the matrix elements used in the computations are shown in the Appendix. Finally, the vectors $\boldsymbol{I}$ (equals the $i$th column of $[Y]$), $\boldsymbol{J}$, $\boldsymbol{J}^f$, and $\boldsymbol{K}^f$ can be determined by solving the matrix equations (7) with the aid of a digital computer.

## III. Numerical Results for Three-Port Circulators

### A. Y Junction with a Central Circular Ferrite Post

For comparison with the previously published experimental and theoretical results, we first treat Y-junction circulators with a central circular ferrite post. The circulator performances using two different ferrite samples, that is, TT1-109 ($4\pi M_s = 1317$ G, $\epsilon_r = 11.7$, $\Delta H = 135$ Oe, and the radius of the ferrite post, $r$ equals 3.50 mm) and G-1002 ($4\pi M_s = 1000$ G, $\epsilon_r = 15.4$, $\Delta H = 100$ Oe, and $r = 3.00$ mm) have been calculated and are shown in Figs. 2 and 3, respectively. Here $4\pi M_s$ is the saturation magnetization, $\Delta H$ is the resonance line width, and the internal dc magnetic field $H_0$ equals 200 Oe. Note that the loss of the ferrites is not neglected in these computations. The experi-

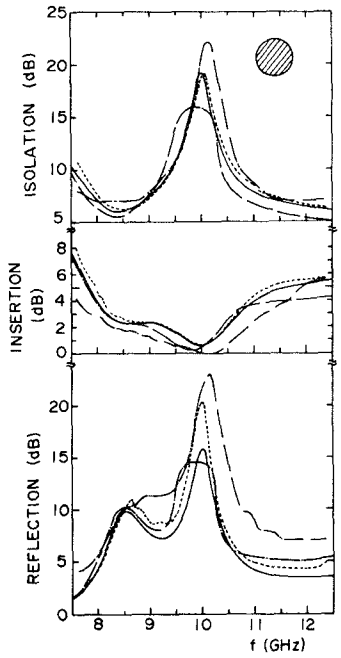


Fig. 2. Frequency responses of circulator with TT1-109 circular ferrite post: ——— values obtained by present theory, ---- measured values given by [5], ——·—— computed values by point-matching technique [7], and ——··—— computed values given by [5].

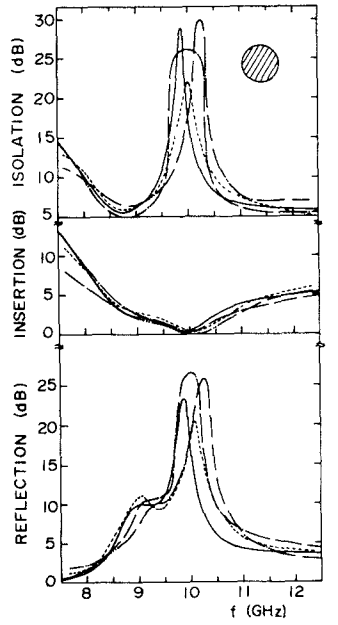


Fig. 3. Frequency responses of circulator with G-1002 circular ferrite post: ——— values obtained by present theory, ---- measured values given by [5], ——·—— computed values by point-matching technique [7], and ——··—— computed values given by [5].

mental results of Castillo and Davis [5] and their numerical results using the field analysis of Davies [2] were read directly from their figures and are plotted together in Figs. 2 and 3. Moreover, the numerical results of the point-matching method [7] are also shown in the same figures. In Fig. 2 the value of the maximum isolation obtained by the present method is $-19.2$ dB at the frequency $f=9.98$ GHz, and that is found to be very close to the measured

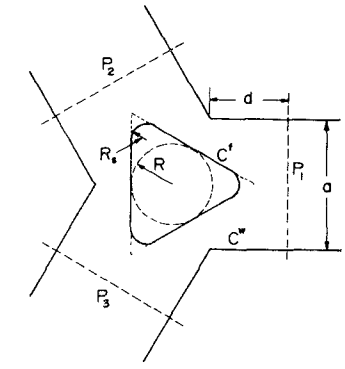


Fig. 4. Symmetrical three-port circulator with triangular ferrite cylinder whose angles are rounded off.

value. In Fig. 3 the agreement with the measured value is not so good as in Fig. 2. The isolation becomes the maximum value $-28.9$ dB at $f=9.87$ GHz. However, in comparison with the other theoretical curves, the present method is found to give the fairly good results close to the experimental results on the whole.

Recently, Castillo and Davis [6] improved the accuracy of their numerical results by adding more modes in the junction and the waveguides.

### *B. Y Junction with a Triangular Ferrite Post Having Rounded Angles*

Consider now a Y junction with a triangular ferrite post whose angles are rounded off (the radius is $R_s$) as shown in Fig. 4. The geometry of the ferrite is specified by the radius $R$ of the inscribed circle of the triangle and by the ratio $\nu$ of the length of circular arcs to that of straight lines of contour $C^f$. When $\nu$ equals zero and infinity, contour $C^f$ reduces to a regular triangle and a circle, respectively. The ferrite material used for the calculations is YIG ($4\pi M_s = 1000$ G, $\epsilon_r = 14$, and $\Delta H = 50$ Oe), that is, Y14 produced by Fuji Electrochemical Company, Ltd. It was found for this sample with small $\Delta H$ that the isolation slightly meliorated and the reflection slightly deteriorated in the neighborhood of the respective maxima of the performance curves in comparison with the case of $\Delta H = 0$. Therefore, the ferrite loss is neglected in the following numerical results.

First, we illustrate the convergence of the solutions. As the junction is loss-free, the scattering matrix $[S]$ derived from the admittance matrix $[Y]$ must be unitary. Therefore, we examine the matrix norm [15] $\|e\| = \max_i \sum_j |e_{ij}|$ where $e_{ij}$ is an element of the matrix $[e]=[S^{t*}][S]-[I]$, the superscript $t$ denotes the transposed matrix, and $[I]$ is a unit matrix. Fig. 5 plots the norm $\|e\|$ versus the partition number $N^f$ of contour $C^f$ for the ferrite post of $R=2.75$ mm and $\nu=1$ where $H_0=700$ Oe, $f=9.6$ GHz, and $a=22.9$ mm. It is seen that for the respective values of $d$ (the distance from the reference plane to the junction), the norm decreases with increase of the partition number. Moreover, the individual elements of $[S]$ were found to converge to constant values. However, $d=10$ mm is found

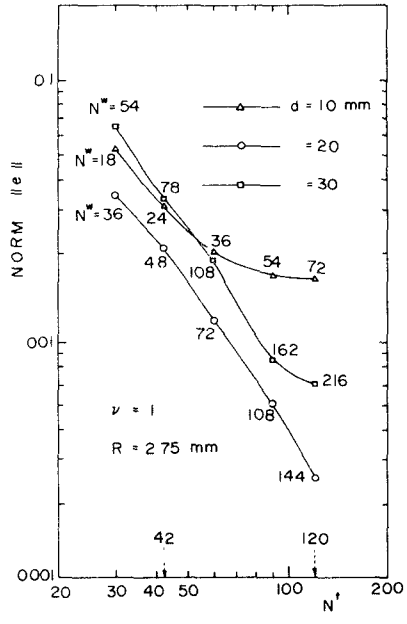


Fig. 5. Norm $\|e\|$ of matrix $[e]=[S^{t*}][S]-[I]$ versus partition number $N^f$ of ferrite air boundary.

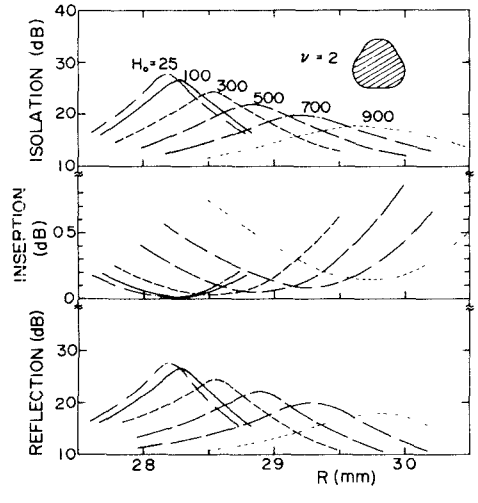


Fig. 6. Performance of circulator with ferrite post of $\nu=2$ versus $R$ at $f=9.6$ GHz.

to be too short to give good convergence, for the higher modes excited in the junction are still significant at the reference planes. The best convergence is obtained in the case of $d=20$ mm and, hence, we select $d=20$ mm in the following numerical results.

Figs. 6–8 show the performance of the junction circulators including the ferrite posts of $\nu=2$, 1/2, and 1/4, respectively, as functions of the radius $R$ with $H_0$ as a parameter where $f=9.6$ GHz. That is to say, the influences of both the magnetic field $H_0$ and the ferrite geometry on the performance of the circulators are illustrated. Since the circulators are assumed free of any dissipation, all calculated losses are due to scattering to the unwanted ports. There is a close resemblance between the curves of the isolation and reflection coefficient. The axis of abscissa in Figs. 6–8 is the radius $R$ of the

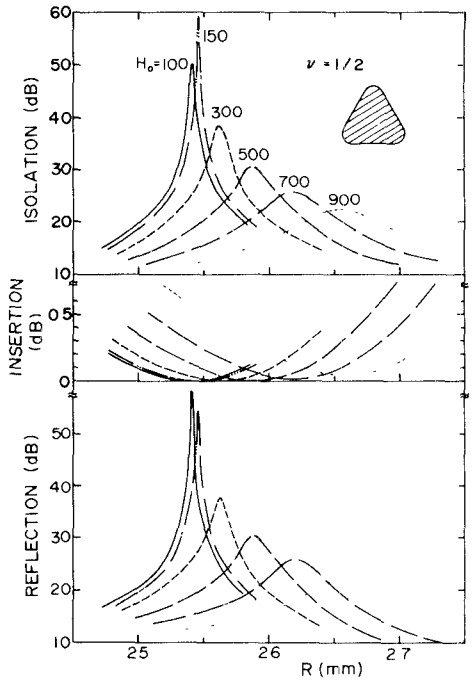


Fig. 7. Performance of circulator with ferrite post of $\nu=1/2$ versus $R$ at $f=9.6$ GHz.

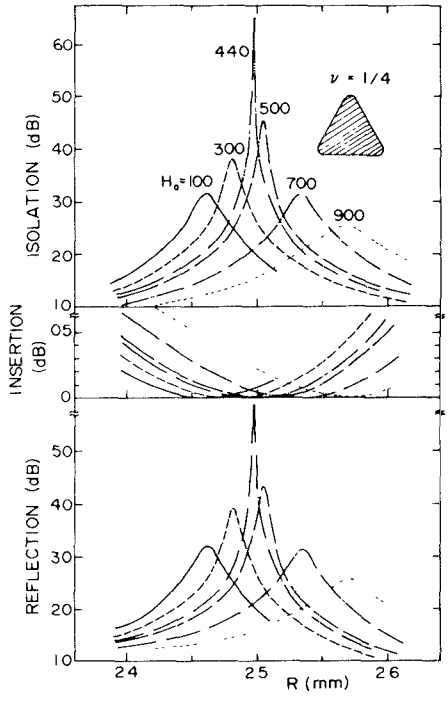


Fig. 8. Performance of circulator with ferrite post of $\nu=1/4$ versus $R$ at $f=9.6$ GHz.

inscribed circle of the triangle as in Fig. 4, and, hence, the ferrite geometry with the same value of $\nu$ similarly grows larger with increase of $R$. From the figures it is seen that, for a given $H_0$, there is only one value of $R$ $(=R_{max})$ which yields the maximum isolation, and that $R_{max}$ tends to increase with increases of $H_0$ and $\nu$. Moreover, it is shown that for constant values of $R$ and $\nu$, that is, the ferrite post of the same geometry, the isolation peaks for a

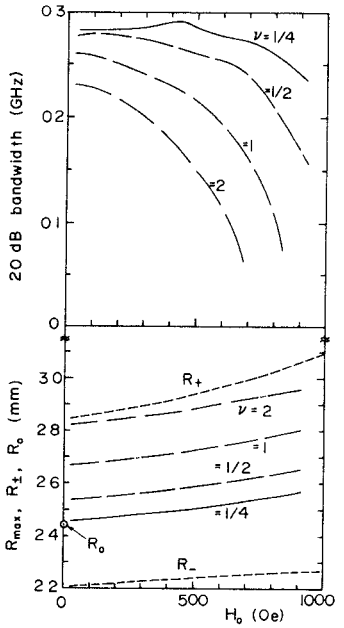


Fig. 9. Radii $R_{max}$ of triangular ferrite which yield maximum isolation, and radii $R_{\pm}, R_0$ of circular ferrite for counter-rotating normal modes versus applied magnetic field. 20-dB bandwidths for ferrite post of $R=R_{max}$ are also shown.

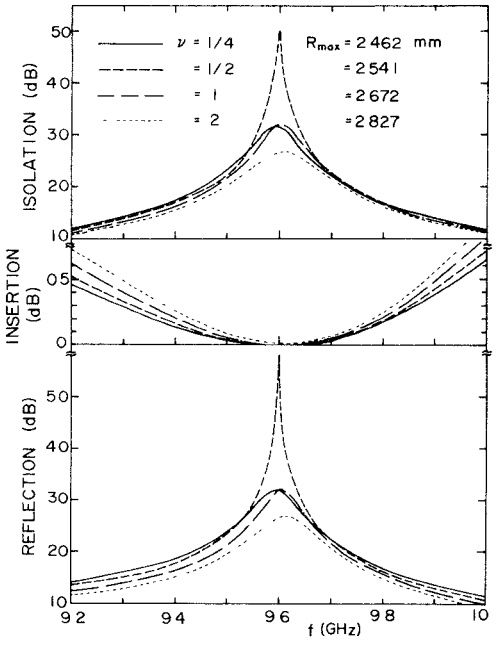


Fig. 10. Frequency responses of circulators including ferrites of $R=R_{max}$ with respective values of $\nu$ at $H_0=100$ Oe.

suitable applied field. Fig. 9 plots the value of $R_{max}$ versus $H_0$ with $\nu$ as a parameter. For comparison, we also illustrate the radii $R_{\pm}$ of the circular ferrite when the counter-rotating normal modes [16] $E_z=A_{\pm}J_1(k_f R_{\pm})e^{\mp j\phi}$ are resonant at the lowest roots resulting from the boundary condition $H_\phi=0$ on the ferrite surface. Here $J_1$ is the Bessel function of order one. Moreover, the radius $R_0$ of the nonmagnetized circular ferrite resonating at the same modes is shown. It is seen that the radius $R_{max}$ calculated lies between $R_+$ and $R_-$. Fig. 9 also shows the 20-dB bandwidth versus $H_0$ when $R=R_{max}$. Note that each curve is not for the ferrite post of the same geometry, but for that of $R=R_{max}$ which gives the maximum isolation for the respective values of $H_0$. It is found that, within the range of $H_0=25$–$900$ Oe, the calculated 20-dB bandwidth is greater for the ferrite post with the smaller value of $\nu$. This result coincides with the indication by Fay and Comstock [16] that the use of a triangular-shaped ferrite contributes to the broad-banding of circulators. Fig. 10 gives the frequency responses of the circulators for the case of $R=R_{max}$ and $H_0=100$ Oe. Excepting the neighborhood of the center frequency at $\nu=1/2$, it is found that the better performance is obtained with decrease of $\nu$.

## IV. Conclusions

Simultaneous matrix equations are given for solving the problem of $H$-plane waveguide junctions with a full-height ferrite post of arbitrary shape. Using the matrix equations, we first deal with Y-junction circulators with a circular ferrite post for comparison with the published experimental and theoretical results. The present method is found to give the fairly good results close to the experimental results on the whole. We next examine the properties of Y-junction circulators with a triangular ferrite post having rounded angles, that is, the influences of both the magnetic field and the ferrite geometry on the performance. It is found that the calculated 20-dB bandwidth becomes greater as the cross section of the ferrite approaches a regular triangle from a circle.

The present method can be extended to the problems of various waveguide junctions with composite gyrotropic cylinders including metals and dielectrics.

## Appendix

In order to express concisely the matrix elements of (8) and (9), we place the coordinate origin at the midpoint of the $i$th port $P_i$ so that $\hat{n}$ and $\hat{l}$ on $P_i$ coincide with $\hat{y}$ and $-\hat{x}$, respectively, where $\hat{x}$ and $\hat{y}$ are unit vectors directed to the $x$ and $y$ axes. Equations (8) and (9) are then written down as

$$G^s_{im}=-j(k\bar{y}^s_m/4)\int_{-a/2}^{a/2}\cos\frac{\pi x}{a}\cdot H_1^{(2)}(k|\hat{x}x-\bar{r}^s_m|)/|\hat{x}x-\bar{r}^s_m|\cdot dx, \qquad s\neq p, \quad i\neq m$$

$$G^p_{ii}=-1/2 \tag{15}$$

$$E^{sp}_{mn}=-(kz_0/4)\int_{-a/2}^{a/2}\cos\frac{\pi x}{a}\cdot H_0^{(2)}(k|\hat{x}x-\bar{r}^s_m|)\,dx, \qquad s\neq p, \quad m\neq n$$

$$E^{pp}_{mm}=-U(k\Delta^p)-(kz_0/2)\int_{\Delta^p/2}^{a/2}\cos\frac{\pi x}{a}\cdot H_0^{(2)}(kx)\,dx \tag{16}$$

where

$$U(k\Delta^p)=j\frac{k\Delta^p z_0}{2\pi}\left\{f(k\Delta^p)+1-\frac{(k\Delta^p)^2}{48}\left[f(k\Delta^p)-\frac{2}{3}-\frac{3(k\Delta^p)^2}{320}(f(k\Delta^p)-1.3)\right]\right\}$$

$$f(k\Delta^p)=\ln(4/k\Delta^p)-\gamma-j\pi/2, \qquad z_0=(\mu_0/\epsilon_0)^{1/2}$$
$$\gamma=0.5772156649\cdots. \quad (17)$$

Moreover, $\bar{r}_m^s=\hat{x}\bar{x}_m^s+\hat{y}\bar{y}_m^s$, $H_1^{(2)}$ is the Hankel function of order one, and $\Delta^p$ is the arc length of a subsection whose location is selected on $P_i$, including the coordinate origin.

Similarly, we obtain the following expressions from (10)–(14):

$$E_{mn}^{sw}=(kz_0/4)\int_{\Delta C_n^w}H_0^{(2)}(k|\boldsymbol{r}-\bar{r}_m^s|)\,dl, \qquad s\neq w, \qquad m\neq n$$
$$E_{mm}^{ww}=U(k\Delta^w) \quad (18)$$

$$E_{mn}^{sf}=(kz_0/4)\int_{\Delta C_n^f+\Delta C_{n+1}^f}T_n(\boldsymbol{r})H_0^{(2)}(k|\boldsymbol{r}-\bar{r}_m^s|)\,dl, \qquad s\neq f, \qquad m\neq n$$
$$E_{mm}^{ff}=V(k\Delta^f) \quad (19)$$

$$H_{mn}^{sf}=-\frac{ik}{4}\int_{\Delta C_n^f+\Delta C_{n+1}^f}T_n(\boldsymbol{r})\frac{\hat{n}\cdot(\boldsymbol{r}-\bar{r}_m^s)}{|\boldsymbol{r}-\bar{r}_m^s|}H_1^{(2)}(k|\boldsymbol{r}-\bar{r}_m^s|)\,dl, \qquad s\neq f, \qquad m\neq n$$
$$H_{mm}^{ff}=1/2+W_m(k\Delta^f) \quad (20)$$

$$\hat{E}_{mn}^{ff}=(kz_0\mu_{\text{eff}}/4\mu_0)\int_{\Delta C_n^f+\Delta C_{n+1}^f}T_n(\boldsymbol{r})H_0^{(2)}(k_f|\boldsymbol{r}-\bar{r}_m^f|)\,dl, \qquad m\neq n$$
$$\hat{E}_{mm}^{ff}=(k\mu_{\text{eff}}/k_f\mu_0)V(k_f\Delta^f) \quad (21)$$

$$\hat{H}_{mn}^{ff}=-\frac{ik_f}{4}\int_{\Delta C_n^f+\Delta C_{n+1}^f}T_n(\boldsymbol{r})\frac{(\hat{n}-j\mu_q\hat{l})\cdot(\boldsymbol{r}-\bar{r}_m^f)}{|\boldsymbol{r}-\bar{r}_m^f|}\cdot H_1^{(2)}(k_f|\boldsymbol{r}-\bar{r}_m^f|)\,dl, \qquad m\neq n$$
$$\hat{H}_{mm}^{ff}=-1/2+W_m(k_f\Delta^f). \quad (22)$$

Here

$$V(k\Delta^f)=j\frac{k\Delta^f z_0}{2\pi}\left\{h(k\Delta^f)+\frac{3}{2}-\frac{(k\Delta^f)^2}{24}\cdot\left[h(k\Delta^f)-\frac{5}{12}-\frac{(k\Delta^f)^2}{40}\left(h(k\Delta^f)-\frac{34}{30}\right)\right]\right\}$$

$$W_m(k\Delta^f)=\frac{\beta_m}{4\pi}\left\{1+\frac{(k\Delta^f)^2}{12}\cdot\left[h(k\Delta^f)+\frac{13}{12}-\frac{(k\Delta^f)^2}{20}\left(h(k\Delta^f)+\frac{97}{60}\right)\right]\right\}$$

$$h(k\Delta^f)=\ln(2/k\Delta^f)-\gamma-j\pi/2 \quad (23)$$

where $\Delta^w$ is the arc length of the subsections on $C^w$ and $\beta_m$ is the angle subtending the circular arc which approximates to the subsection $\Delta C_m^f$. Note that the respective second equations of (20) and (22) hold good in case of $\beta_{m+1}=\beta_m$. Therefore, for the geometry as in Fig. 4, slight modifications are required at the boundaries of circular arcs and straight lines where $\beta_{m+1}\neq\beta_m$. The angle $\beta_m$ is reduced to zero for the subsections on the straight lines. The definite integrals in the above expressions are calculated by numerical integration.

## Acknowledgment

The author is greatly indebted to Prof. R. Yamada and Prof. K. Fujisawa for their criticisms and encouragements. He also wishes to thank T. Tsukamoto for his assistance in numerical computations. The numerical calculations were performed on the HITAC 8800/8700 at University of Tokyo.

## References

[1] H. N. Chait and T. R. Curry, "Y circulator," *J. Appl. Phys.*, vol. 30, p. 152, Apr. 1959.
[2] J. B. Davies, "An analysis of the *m*-port symmetrical *H*-plane waveguide junction with central ferrite post," *IRE Trans. Microwave Theory Tech.*, vol. MTT-10, pp. 596–604, Nov. 1962.
[3] ——, "Theoretical design of wideband waveguide circulators," *Electron. Lett.*, vol. 1, pp. 60–61, May 1965.
[4] C. G. Parsonson, S. R. Longley, and J. B. Davies, "The theoretical design of broad-band 3-port waveguide circulators," *IEEE Trans. Microwave Theory Tech.*, vol. MTT-16, pp. 256–258, Apr. 1968.
[5] J. B. Castillo, Jr., and L. E. Davis, "Computer-aided design of three-port waveguide junction circulators," *IEEE Trans. Microwave Theory Tech.*, vol. MTT-18, pp. 25–34, Jan. 1970.
[6] ——, "A higher order approximation for waveguide circulators," *IEEE Trans. Microwave Theory Tech.*, vol. MTT-20, pp. 410–412, June 1972.
[7] M. E. El-Shandwily, A. A. Kamal, and E. A. F. Abdallah, "General field theory treatment of *H*-plane waveguide junction circulators," *IEEE Trans. Microwave Theory Tech.*, vol. MTT-21, pp. 392–403, June 1973.
[8] A. Khilla and I. Wolff, "Field theory treatment of *H*-plane waveguide junction with triangular ferrite post," *IEEE Trans. Microwave Theory Tech.*, vol. MTT-26, pp. 279–287, Apr. 1978.
[9] K. K. Mei and J. G. Bladel, "Scattering by perfectly-conducting rectangular cylinders," *IEEE Trans. Antennas Propagat.*, vol. AP-11, pp. 185–192, Mar. 1963.
[10] R. F. Harrington, *Field Computation by Moment Methods*. New York: Macmillan, 1968.
[11] T. Okoshi and S. Kitazawa, "Computer analysis of short-boundary planar circuits," *IEEE Trans. Microwave Theory Tech.*, vol. MTT-23, pp. 299–306, Mar. 1975.
[12] N. Okamoto, "Matrix formulation of scattering by a homogeneous gyrotropic cylinder," *IEEE Trans. Antennas Propagat.*, vol. AP-18, pp. 642–649, Sept. 1970.
[13] N. Okamoto and T. Kimura, "A method for problems of scattering by gyrotropic composite cylinders," *J. Inst. Electron. Commun. Eng. Jap.*, vol. 58-B, pp. 269–276, June 1975.
[14] R. F. Harrington, *Time-Harmonic Electromagnetic Fields*. New York: McGraw-Hill, 1961, pp. 100–103.
[15] V. N. Faddeeva, *Computational Methods of Linear Algebra*. New York: Dover, 1959, pp. 54–62.
[16] C. E. Fay and R. L. Comstock, "Operation of the ferrite junction circulator," *IEEE Trans. Microwave Theory Tech.*, vol. MTT-13, pp. 15–27, Jan. 1965.